

Scaling Properties in Transistors That Use Aligned Arrays of Single-Walled Carbon Nanotubes

Xinning Ho,[†] Lina Ye,[†] Slava V. Rotkin,[†] Qing Cao,[§] Sakulsuk Unarunotai,[§] Shuaib Salamat,^{||} Muhammad A. Alam,^{||} and John A. Rogers^{†,§,⊥,*}

[†]Departments of Materials Science and Engineering, Beckman Institute, and Frederick Seitz Materials Research Laboratory, University of Illinois at Urbana–Champaign, 1304 West Green Street, Urbana, Illinois 61801,

[‡]Department of Physics, Lehigh University, Bethlehem, Pennsylvania 18015, and Centre for Advanced Materials and Nanotechnology, Lehigh University, Bethlehem, Pennsylvania 18015, [§]Department of Chemistry, University of Illinois at Urbana–Champaign, Urbana Illinois 61801, ^{||}Department of Electrical and Computer Engineering, Purdue University, 465 Northwestern Avenue, West Lafayette, Indiana 47907, and [⊥]Department of Electrical and Computer Engineering, Mechanical Science and Engineering, University of Illinois at Urbana–Champaign, Urbana, Illinois 61801

ABSTRACT Recent studies and device demonstrations indicate that horizontally aligned arrays of linearly configured single-walled carbon nanotubes (SWNTs) can serve as an effective thin film semiconductor material, suitable for scalable use in high-performance transistors. This paper presents the results of systematic investigations of the dependence of device properties on channel length, to reveal the role of channel and contact resistance in the operation. The results indicate that, for the range of channel lengths and SWNT diameters studied here, source and drain contacts of Pd yield transistors with effectively Ohmic contacts that exhibit negligible dependence of their resistances on gate voltage. For devices that use Au, modulation of the resistance of the contacts represents a significant contribution to the response. Extracted values of the mobilities of the semiconducting SWNTs and the contact resistances associated with metallic and semiconducting SWNTs are consistent with previous reports on single tube test structures.

KEYWORDS Carbon nanotube, transistor, radio frequency, gigahertz, quartz

Submonolayer collections of single-walled carbon nanotubes (SWNTs) represent attractive semiconductor materials for effective, thin film type transistors (TFTs)¹ partly because the mobilities of individual SWNTs can approach 10000 cm²/(V s),² and possibly higher, significantly exceeding that of silicon. Arrays or networks of SWNTs provide a scalable way to exploit these properties, as well as their excellent mechanical and thermal characteristics. In the case of long channel TFTs that use networks of SWNTs, scaling studies show clearly that the device operation is based on field effect modulation of the properties of the channel; the role of the contacts is experimentally negligible for channel lengths that are large compared to the average lengths of the SWNTs because tube/tube contact resistances dominate the transport.¹ Attractive device-level properties that can be obtained with networks create interest in their use as alternatives to other thin film materials for flexible electronics,³ flat panel electronics, and related systems. Arrays provide much better performance than networks, thereby creating opportunities in analog electronics^{4,5} and other areas where the performance requirements can be demanding. Average tube densities up to 10 SWNTs/ μm

have been achieved in arrays with nearly perfect degrees of alignment by guided growth on quartz. In certain areas, the tube density can be up to 50 SWNT/ μm , which suggests that improvements in average tube density could be possible with optimization.²² In the case of arrays, it is known that the contacts can greatly influence device operation,^{1,4,6–8} just as with transistor test structures based on individual SWNTs.^{9–11} In the present paper, we study the dependence of device parameters in array-based transistors on channel length in the micrometer range, for cases where the source and drain electrodes consist of Pd and Au. The results indicate that, for arrays with a range of diameters centered at ~ 1.2 nm, the contacts contribute significant, but largely gate-independent resistance in the case of Pd and gate-dependent behavior in the case of Au. The results provide key insights into the behavior of the devices, the scaling of their properties, and directions for future work.

Figure 1a shows a schematic illustration of a TFT that uses a “perfectly” aligned parallel array of single-walled carbon nanotubes (SWNTs) for the semiconductor and a scanning electron microscope (SEM) image of an array representative of the type used here. The SWNTs were grown directly into such configurations via chemical vapor deposition (CVD) on an ST (stable temperature) cut quartz substrate, using procedures described elsewhere.¹² The devices studied here used two different metallization schemes for the source and drain elec-

* To whom correspondence should be addressed. jrogers@uiuc.edu.

Received for review: 10/1/2009

Published on Web: 01/05/2010

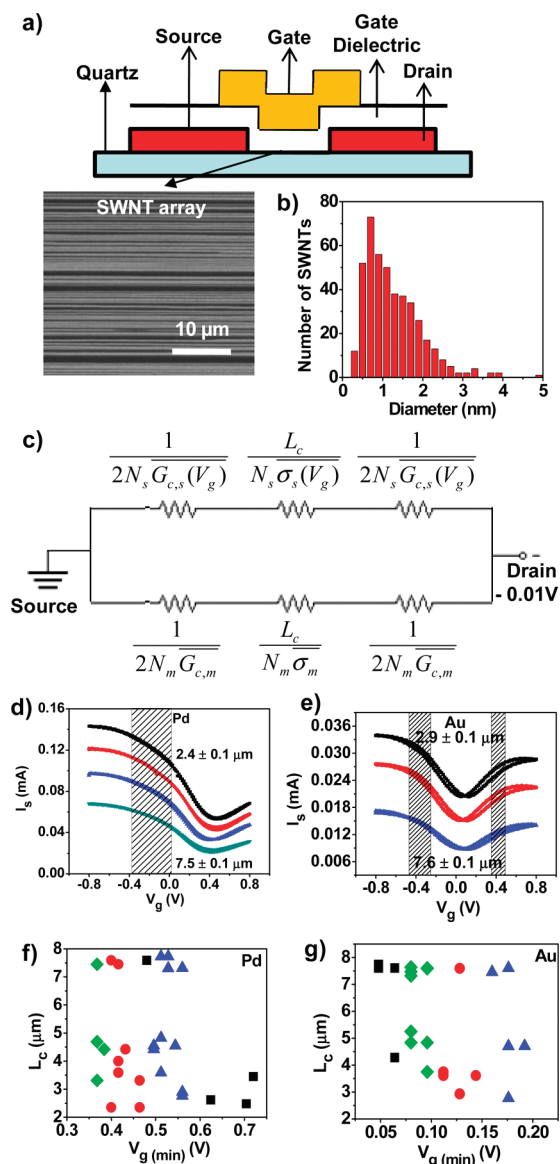


FIGURE 1. (a) Schematic illustration of a single-walled carbon nanotube (SWNT) array transistor with an SEM image of a representative array in the frame below. (b) Typical diameter distribution of SWNTs measured by AFM. (c) Equivalent circuit model for a device with channel length L_c , showing the resistances contributed by the inverse of the average conductances of the contacts to the semiconducting and metallic SWNTs (i.e., $1/\bar{G}_{c,s}$ and $1/\bar{G}_{c,m}$), respectively) and the role of the SWNTs in transport through the channel (i.e., $L_c/\bar{\sigma}_s$ and $L_c/\bar{\sigma}_m$). The numbers of s-SWNT and m-SWNT are N_s and N_m , respectively. Representative transfer curves of (d) Pd and (e) Au electrode devices with channel width (W) = 400 μm at $V_d = -0.01$ V. The channel lengths of the Pd devices are 2.4 ± 0.1 μm (black symbols), 4.4 ± 0.1 μm (red symbols), 4.4 ± 0.1 μm (blue symbols), and 7.5 ± 0.1 μm (green symbols) from top to bottom. The channel lengths of the Au devices are 2.9 ± 0.1 μm (black symbols), 3.7 ± 0.1 μm (red symbols), and 7.6 ± 0.1 μm (blue symbols) from top to bottom. The highlighted regions show the range of V_g values that were analyzed. The bottom frames show combinations of L_c and gate voltages at minimum current ($V_{g(\min)}$), for (f) Pd and (g) Au devices. The devices that form the focus of the analysis are shown in red. Two other clusters of devices, indicated in blue and green, were also analyzed.

trodes, both defined by photolithography and liftoff directly on the arrays. In one case, the metal was Pd (30 nm)/Ti (1 nm); in the other it was Au (30 nm)/Ti (1 nm). Layers of hafnium oxide (HfO₂) deposited on top of the resulting structures formed the gate dielectrics (94 ± 7 nm in the case of Pd/Ti; 128 ± 3 nm in the case of Au/Ti). Gate electrodes (Au (30 nm)/Ti (2 nm)) aligned to the channels, but significantly overlapping (by ~ 20 μm) both the source and drain, were defined by photolithography and liftoff to complete the devices.

Parts d and e of Figure 1 show typical transfer curves of devices with Pd and Au electrodes, respectively, measured with the source grounded, the drain held at a bias of -0.01 V, and the gate bias swept between ± 0.8 V. The Pd devices display predominantly p-type behavior while the Au transistors show ambipolar characteristics, both with only small levels of hysteresis. This outcome is consistent with the lower work function of Au and reduced barrier for electron injection, compared to Pd. The densities of the arrays (measured in tubes per micrometer of lateral distance across the channel) were 4 ± 0.5 SWNTs/μm for Pd and 2 ± 0.5 SWNTs/μm for Au, as determined by the average of SEM measurements at various spots across the surface of the substrate. Figure 1b shows a typical diameter distribution of the SWNTs. The diameters are critically important to the behavior of the devices, as the band gaps of the SWNTs and their mobilities depend strongly on this parameter.^{2,13} Also, experimental studies of test structures that use individual SWNTs indicate that Schottky barriers at the contacts and threshold behavior vary strongly with diameter.¹¹ Statistical averaging associated with the arrays reduces but does not eliminate variability in device properties associated with slightly different diameter distributions of the incorporated SWNTs, as confirmed by theoretical studies on arrays with different diameter distributions.¹⁴ To minimize the influence of such effects, we separately analyzed collections of devices that exhibited minimum current outputs at similar gate voltages, such as those presented in parts d and e of Figure 1, as a proxy for similar diameter distributions and contact properties. This procedure also, at the same time, removes device to device variations that can be caused by other effects, such as different amounts of residual charge in or near the channel. Parts f and g of Figure 1 plot the combinations of channel lengths and gate voltages at minimum current, for Pd and Au devices, respectively. The devices that form the focus of the results presented in the following are highlighted in red, where the minimum current voltage for the Pd and Au devices are ~ 0.43 and ~ 0.13 V, respectively. Separate analysis was also performed on two other clusters of devices, as highlighted in blue and green in parts f and g of Figure 1. Summaries of results for analysis of these collections of devices, which we will refer to as blue and green clusters of devices, are also provided. In all of the following, we assume that the ratio of m-SWNTs to s-SWNTs is 1:2 and that $\sim 80\%$ of all of these SWNTs bridge the source and drain.⁴

We analyzed the behavior using a simple equivalent circuit model, as shown in Figure 1c, in which we assume diffusive transport in the channel. We refer to the number of semiconducting (s-SWNT) and metallic (m-SWNT) tubes bridging the source and drain as N_s and N_m . The resistance of a given tube, with index i , is $R_s^{(i)}$ and $R_m^{(i)}$, for s-SWNT and m-SWNT, respectively. As measured in the TFT structure, the resistance of each SWNT has two components: (i) a contact resistance ($R_{c,s}^{(i)}$ and $R_{c,m}^{(i)}$ for s-SWNT and m-SWNT, respectively) at the source and the drain electrodes and (ii) a channel resistance determined by the product of the channel length, L_c , and the resistivity (i.e., resistance per unit length), $\rho_s^{(i)}$ and $\rho_m^{(i)}$, of s-SWNT and m-SWNT, respectively. The resistances of the transport pathways associated with each of the tubes add in parallel, due to the array geometry. The total resistance of the TFT device (R_{tot}), then, can be written as the following, where the dependencies on gate voltage (V_g) are indicated explicitly

$$\frac{1}{R_{tot}(V_g)} = \sum_{i=1}^{N_s} \frac{1}{R_s^{(i)}(V_g)} + \sum_{i=1}^{N_m} \frac{1}{R_m^{(i)}} = N_s \bar{G}_s(V_g) + N_m \bar{G}_m \quad (1)$$

The quantities $\bar{G}_s(V_g)$ and \bar{G}_m are the average conductances associated with the s-SWNTs and m-SWNTs and their contacts to the source/drain electrodes, respectively, with

$$R_m^{(i)} = \frac{1}{G_m^{(i)}} = R_{c,m}^{(i)} + \rho_m^{(i)} L_c = \frac{1}{G_{c,m}^{(i)}} + \frac{L_c}{\sigma_m^{(i)}} \quad (2)$$

and

$$R_s^{(i)}(V_g) = \frac{1}{G_s^{(i)}(V_g)} = R_{c,s}^{(i)}(V_g) + \rho_s^{(i)}(V_g) L_c = \frac{1}{G_{c,s}^{(i)}(V_g)} + \frac{L_c}{\sigma_s^{(i)}(V_g)} \quad (3)$$

where the G values are the corresponding conductances and σ are the conductivities. As indicated in these equations, the analysis assumes that only $\rho_m^{(i)}$ and $R_{c,m}^{(i)}$ are independent of V_g . We note, however, that it is well-known that even nominally m-SWNTs can often be modulated by an applied field, due possibly to defects or other nonideal aspects.¹⁵

With these expressions, intrinsic properties can be extracted from the electrical properties and their dependence on L_c . First, we associate the minimum current (I_{off}) extracted from the transfer curves with transport, approximately,

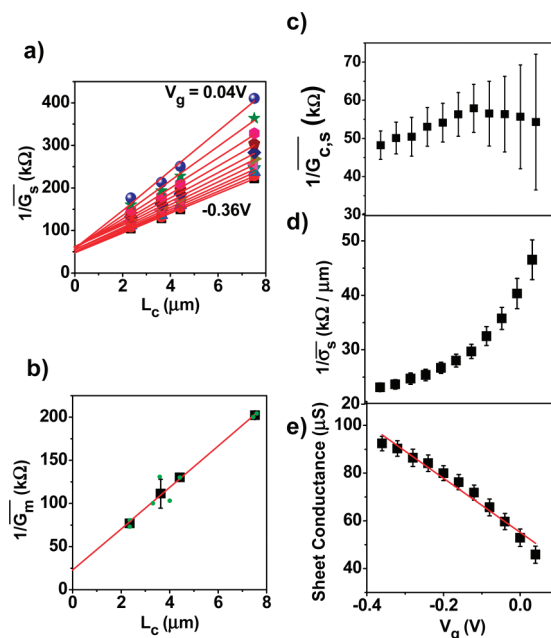


FIGURE 2. Channel length scaling and extracted intrinsic properties of Pd devices. (a) The inverse of the average conductance of the s-SWNTs ($1/\bar{G}_s$) as a function of channel length (L_c) at gate voltages (V_g) of 0.04 V (blue circles), 0 V (green stars), -0.04 V (pink hexagons), -0.08 V (brown pentagons), -0.12 V (blue diamonds), -0.16 V (light green triangles), -0.20 V (pink triangles), -0.24 V (dark green triangles), -0.28 V (blue triangles), -0.32 V (red circles), and -0.36 V (black squares) from top to bottom. (b) The inverse of the average conductance of the m-SWNTs ($1/\bar{G}_m$) as a function of channel length. The black squares with error bars represent the average of individual devices (green circles). (c) Inverse of the average conductance of the contact of the s-SWNTs ($1/\bar{G}_{c,s}$) extracted from the intercept in (a) as a function of gate voltage. (d) Inverse of the average conductivity of the s-SWNTs ($1/\bar{\sigma}_s$) extracted from the slope in (a) as a function of gate voltage. (e) Sheet conductance of the s-SWNTs as a function of gate voltage.

through the m-SWNTs. We refer to the resistance at this minimum as the off-state resistance, R_{off} . Using Ohm's law, we can write

$$\frac{1}{R_{off}} = \frac{I_{off}}{V_d} = \sum_{i=1}^{N_m} \frac{1}{R_m^{(i)}} = N_m \bar{G}_m \quad (4)$$

where V_d is the drain bias (-0.01 V). Next, we associate the difference between current measured at a given V_g , $I_{on}(V_g)$ and I_{off} , which we refer to as I_{on-off} , with transport through the s-SWNT. Again, using Ohm's law

$$\frac{1}{R_{on-off}} = \frac{I_{on-off}}{V_d} = \sum_{i=1}^{N_s} \frac{1}{R_s^{(i)}(V_g)} = N_s \bar{G}_s(V_g) \quad (5)$$

Parts a and b of Figure 2 show the dependence of $1/\bar{G}_s(V_g)$ and $1/\bar{G}_m$ of transistors with palladium electrodes on L_c ,

respectively. The extracted $1/\bar{G}_{c,m}$ for the m-SWNTs is small, $\sim 20 \pm 5 \text{ k}\Omega$, comparable to values from earlier reports ($\sim 14 \text{ k}\Omega$)^{16,17} and between values obtained from analysis of the blue (not fitted to a finite value within statistical accuracy) and green ($\sim 56 \text{ k}\Omega$) clusters of Pd devices. The extracted value of $1/\bar{\sigma}_m$ is $24 \pm 5 \text{ k}\Omega/\mu\text{m}$, which lies between previous reports of devices of this type ($\sim 80 \text{ k}\Omega/\mu\text{m}$),⁴ and values reported for individual tube devices ($\sim 6 \text{ k}\Omega/\mu\text{m}$).^{18,19} Likewise, $1/\bar{\sigma}_m$ from similar analysis on the different clusters of devices are also in this range ($\sim 45 \text{ k}\Omega/\mu\text{m}$ for blue; $\sim 20 \text{ k}\Omega/\mu\text{m}$ for green). According to eq 3, linear fits to the data $1/\bar{G}_s(V_g)$ vs L_c yield the inverse of the average conductances of the contacts from the intercepts and the inverse of the average conductivities from the slopes. Parts c and d of Figure 2 plot the dependence of $1/\bar{G}_{c,s}$ and $1/\bar{\sigma}_s$, as a function of V_g , respectively. The results show that $1/\bar{G}_{c,s}$ is $\sim 50 \pm 20 \text{ k}\Omega$, with no significant dependence on V_g , to within experimental uncertainties. This result is quantitatively similar to previous studies of individual tube devices with similar diameters and metallization ($\sim 32 \text{ k}\Omega$).²⁰ Analysis of blue and green Pd devices yields $1/\bar{G}_{c,s}$ values of $\sim 0 \pm 10 \text{ k}\Omega$ and $\sim 50 \pm 20 \text{ k}\Omega$, respectively. In neither case is the contact resistance significantly modulated by V_g . The data of Figure 2d show clearly that $1/\bar{\sigma}_s$ is modulated strongly by V_g . This dependence can be used to extract the average intrinsic mobility, $\bar{\mu}_i$ and the average threshold voltage, \bar{V}_t , of the s-SWNTs from the slope and the intercept of a plot of average sheet conductance ($\Delta L_c/\Delta R_{\text{on-off}}W$) versus V_g (Figure 2e). In particular, in the linear region, where $V_d \ll V_g$, it can be shown that

$$\frac{\Delta L_c}{\Delta R_{\text{on-off}}W} = (\bar{\mu}_i C_w) V_g - \bar{\mu}_i C_w \bar{V}_t \quad (6)$$

where C_w is the specific capacitance per unit area of the TFT device and W is the channel width of the device. The specific capacitance per unit area of the TFT device for an infinite array of parallel SWNTs with uniform spacing $1/D$ that includes the effects of electrostatic screening and fringing fields is given by

$$C_w = \frac{D}{C_Q^{-1} + \frac{1}{2\pi\epsilon_0\epsilon_s} \log \frac{\sinh(2\pi tD)}{\pi R D}} \quad (7)$$

where C_Q^{-1} is the quantum capacitance²¹ ($4 \times 10^{-10} \text{ F} \cdot \text{m}^{-1}$), R is the radius of the SWNTs, t is the distance to the gate electrode, ϵ_s is the dielectric constant of the surface/interface where we place the SWNTs,⁴ and D is the density of the SWNTs. The dielectric constant in the quartz/SWNT/HfO₂ sandwich structure is approximated as $\epsilon_s = (\epsilon_{\text{SiO}_2} + \epsilon_{\text{HfO}_2})/2 = (4 + 16)/2 = 10$. If we take D as corresponding only to the contribution of the s-SWNTs, then we find that $\bar{\mu}_i \sim 5700 \text{ cm}^2/(\text{V s})$, which is in the same range as average values reported previ-

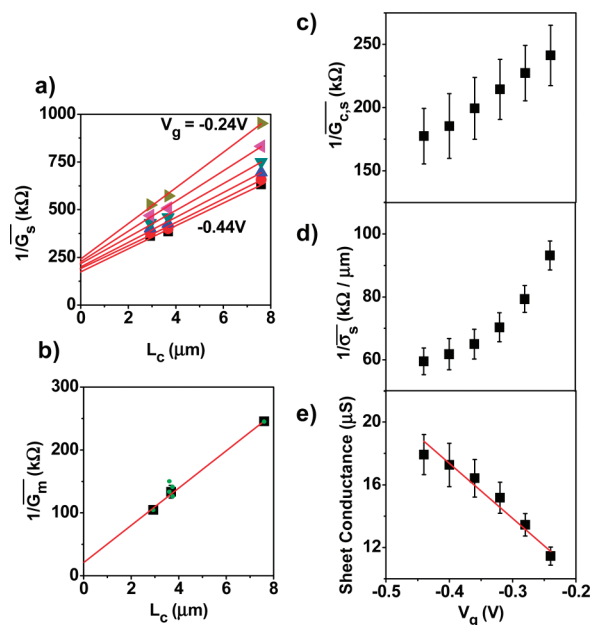


FIGURE 3. Channel length scaling and extracted intrinsic properties of the m-SWNTs and s-SWNTs in the p-channel branch of the gold electrode devices. (a) The inverse of the average conductance of the s-SWNTs ($1/\bar{G}_s$) as a function of channel length (L_c) at gate voltages (V_g) of -0.24 V (light green triangles), -0.28 V (pink triangles), -0.32 V (dark green triangles), -0.36 V (blue triangles), -0.40 V (red circles), and -0.44 V (black squares) from top to bottom. (b) The inverse of the average conductance of the m-SWNTs ($1/\bar{G}_m$) as a function of channel length. The black squares with error bars represent the average of individual devices (green circles). (c) The inverse of the average conductance of the contact of the s-SWNTs ($1/\bar{G}_{c,s}$) extracted from the intercept in (a) as a function of gate voltage. (d) The inverse of average channel conductivity of the s-SWNTs ($1/\bar{\sigma}_s$) extracted from the slope in (a) as a function of gate voltage. (e) Sheet conductance of the s-SWNTs as a function of gate voltage.

ously in array and single tube devices^{2,4,7,22} and between those determined from analysis of blue ($\sim 2300 \text{ cm}^2/(\text{V s})$) and green ($\sim 10000 \text{ cm}^2/(\text{V s})$) devices. The same analysis yields $\bar{V}_t = 0.50 \pm 0.05 \text{ V}$.

Similar analysis was performed on transistors that use Au for source and drain metallization, as shown in Figure 3. Comparable to the Pd case, the red cluster of Au devices yield $1/\bar{G}_{c,m} = \sim 20 \pm 10 \text{ k}\Omega$ and $1/\bar{\sigma}_m = \sim 30 \pm 5 \text{ k}\Omega/\mu\text{m}$. The extracted values of the $1/\bar{G}_{c,m}$ and the $1/\bar{\sigma}_m$ for the other clusters of Au devices are $\sim 50 \pm 10 \text{ k}\Omega$ (blue) and $\sim 20 \pm 5 \text{ k}\Omega$ (green), and $\sim 20 \pm 5$ and $\sim 30 \pm 5 \text{ k}\Omega/\mu\text{m}$, respectively. The s-SWNTs in the p-channel branch, on the other hand, show different behavior. In particular, for Au, $1/\bar{G}_{c,s}$ is, unlike Pd, dependent on V_g . The magnitude increases systematically from ~ 180 to $\sim 240 \text{ k}\Omega$ as V_g increases from -0.44 to -0.24 V . Qualitatively, this behavior is also observed in the blue cluster of Au devices, but not clearly evident in the green devices. Throughout this range, the values are considerably larger than those in the Pd cases. The lower work function of Au and its poorer wetting on SWNTs compared to Pd might explain these differences. These values are also about an order of magnitude larger than single tube devices

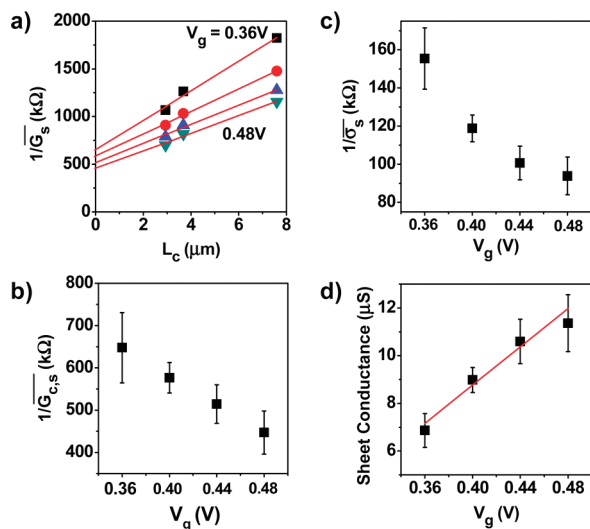


FIGURE 4. Channel length scaling and extracted intrinsic properties of the s-SWNTs in the n -channel branch of the gold electrode devices. (a) The inverse of the average conductance of the s-SWNTs ($1/\bar{G}_s$) as a function of channel length (L_c) at gate voltages (V_g) of 0.36 V (black squares), 0.40 V (red circles), 0.44 V (blue triangles), and 0.48 V (green triangles) from top to bottom. (b) The inverse of average conductance of the contact of the s-SWNTs ($1/\bar{G}_{c,s}$) extracted from the intercept in (a) as a function of gate voltage. (c) The inverse of average channel conductivity ($1/\bar{\sigma}_s$) of the s-SWNTs extracted from the slope in (a) as a function of gate voltage. (d) Sheet conductance of the s-SWNTs as a function of gate voltage.

reported ($\sim 10\text{--}30\text{ k}\Omega$), for diameters of $\sim 3\text{ nm}$ and pure Au electrodes.²⁵ These differences might be caused by different processing conditions, which are known to be extremely important to the behavior of the contacts. The intrinsic mobility of the s-SWNTs extracted from analysis of Au devices is $\sim 3700\text{ cm}^2/(\text{V s})$, comparable to that in the Pd devices. This value is also similar to the values obtained from analysis of the other clusters of devices (i.e., $\sim 2500\text{ cm}^2/(\text{V s})$ for blue; $\sim 2100\text{ cm}^2/(\text{V s})$ for green). The threshold voltage from this analysis is $0.10 \pm 0.05\text{ V}$. The response in the n channel regime operation shows a similar trend. First, the inverse of the average conductance of the contact shows systematic dependence on V_g , decreasing from ~ 650 to $\sim 450\text{ k}\Omega$ as V_g increases from 0.36 to 0.48 V (Figure 4b). Similar results are obtained from analysis of other clusters of devices. We speculate and theoretical work confirms (ref 14) that these behaviors result from the larger Schottky barrier for electrons than holes. The intrinsic mobility observed for electrons is $\sim 4100\text{ cm}^2/(\text{V s})$, similar to that for holes and not too dissimilar from results for the other clusters of Au devices ($3600\text{ cm}^2/(\text{V s})$ for blue; $1600\text{ cm}^2/(\text{V s})$ for green). The threshold voltage from this analysis is $0.2 \pm 0.1\text{ V}$.

In conclusion, systematic studies of channel length scaling in SWNT array transistors show that Pd provides an Ohmic contact to the arrays, with little dependence of resistance on gate voltage. Operation in this case is dominated by modulation of the channel resistance by the gate. Devices with Au, on the other hand, show behavior indicative of gate modulation of both the channel and the contacts,

particularly in the n channel branch. In most cases, quantitative values for the inferred mobilities, SWNT resistances, and contact behaviors are in the same range as those reported previously in single tube test structures and, for certain parameters, in array devices.

Acknowledgment. We thank T. Banks and B. Sankaran for help with processing. This work was carried out in part in the Frederick Seitz Materials Research Laboratory Central Facilities, University of Illinois, which are partially supported by the U.S. Department of Energy under Grants DE-FG02-07ER46453 and DE-FG02-07ER46471. X.H. acknowledges fellowship support from ASTAR (Singapore).

Supporting Information Available. A few representative diameter distributions collected from different parts of the wafer. This material is available free of charge via the Internet at <http://pubs.acs.org>.

REFERENCES AND NOTES

- (1) Cao, Q.; Rogers, J. A. *Adv. Mater.* **2008**, *20*, 29.
- (2) Zhou, X.; Park, J. Y.; Huang, S.; Liu, J.; McEuen, P. L. *Phys. Rev. Lett.* **2005**, *95*, 146805.
- (3) Cao, Q.; Kim, H.-S.; Pimparkar, N.; KulKarni, J. P.; Wang, C.; Shim, M.; Roy, K.; Alam, M. A.; Rogers, J. A. *Nature* **2008**, *454*, 495.
- (4) Kang, S. J.; Kocabas, C.; Ozel, T.; Shim, M.; Pimparkar, N.; Alam, M. A.; Rotkin, S. V.; Rogers, J. A. *Nat. Nanotechnol.* **2007**, *2*, 230.
- (5) Engel, M.; Small, J. P.; Steiner, M.; Freitag, M.; Green, A. A.; Hersam, M. C.; Avouris, P. *ACS Nano* **2008**, *2*, 2445.
- (6) Kocabas, C.; Dunaham, S.; Cao, Q.; Cimino, K.; Ho, X.; Kim, H.-S.; Dawson, D.; Payne, J.; Stuenkel, M.; Zhang, H.; Banks, T.; Feng, M.; Rotkin, S. V.; Rogers, J. A. *Nano Lett.* **2009**, *9*, 1937.
- (7) Ryu, K.; Badmaev, A.; Wang, C.; Lin, A.; Patil, N.; Gomez, L.; Kumar, A.; Mitra, S.; Wong, H. S. P.; Zhou, C. *Nano Lett.* **2009**, *9*, 189.
- (8) Cao, Q.; Rogers, J. A. *Nano Lett.* **2008**, *8*, 259.
- (9) Wind, S. J.; Appenzeller, J.; Avouris, P. *Phys. Rev. Lett.* **2003**, *91*, 58301.
- (10) Appenzeller, J.; Knoch, J.; Derycke, V.; Martel, R.; Wind, S.; Avouris, P. *Phys. Rev. Lett.* **2002**, *89*, 126801.
- (11) Chen, Z.; Appenzeller, J.; Knoch, J.; Lin, Y.-M.; Avouris, P. *Nano Lett.* **2005**, *5*, 1497.
- (12) Kocabas, C.; Hur, S. H.; Gaur, A.; Meitl, M. A.; Shim, M.; Rogers, J. A. *Small* **2005**, *1*, 1110.
- (13) Dresselhaus, M. S.; Dresselhaus, G.; Avouris, P. *Carbon Nanotubes: synthesis, structure, properties and applications*; Springer-Verlag: Berlin, 2001.
- (14) Salamat, S.; Ho, X.; Alam, M. A.; Rogers, J. A. *Intrinsic Performance Variability in Aligned Array CNT Field Effect Transistors*, 2009; submitted.
- (15) Nguyen, K. T.; Shim, M. *J. Am. Chem. Soc.* **2009**, *131*, 7103.
- (16) Kim, W.; Javey, A.; Tu, R.; Cao, J.; Wang, Q.; Dai, H. *Appl. Phys. Lett.* **2005**, *87*, 173101.
- (17) Bachtold, A.; Fuhrer, M. S.; Plyasunov, S.; Forero, M.; Anderson, E. H.; Zettl, A.; McEuen, P. L. *Phys. Rev. Lett.* **2000**, *84*, 6082.
- (18) Javey, A.; Guo, J.; Paulsson, M.; Wang, Q.; Mann, D.; Lundstrom, M.; Dai, H. *Phys. Rev. Lett.* **2004**, *92*, 106804.
- (19) Park, J.-Y.; Rosenblatt, S.; Yaish, Y.; Sazonova, V.; Ustunel, H.; Braig, S.; Arias, A.; Brouwer, P. W.; McEuen, P. L. *Nano Lett.* **2004**, *4*, 517.
- (20) Javey, A.; Guo, J.; Wang, Q.; Lundstrom, M.; Dai, H. *Nature* **2003**, *424*, 654.
- (21) Rosenblatt, S.; Yaish, Y.; Park, J.; Gore, J.; Sazonova, V.; McEuen, P. L. *Nano Lett.* **2002**, *2*, 869.
- (22) Kocabas, C.; Kang, S. J.; Ozel, T.; Shim, M.; Rogers, J. A. *J. Phys. Chem. C* **2007**, *111*, 17879.
- (23) Park, J.-Y.; Yaish, Y.; Rosenblatt, S.; Sazonova, V.; Brink, M.; McEuen, P. L. *Phys. Rev. Lett.* **2004**, *92*, 46401.